



Cite this: DOI: 10.1039/d0nj00213e

In situ synthesis of highly dispersed Co–N–C catalysts with carbon-coated sandwich structures based on defect anchoring†

 Suisheng Li, Lushuang Zhang, Shanshan Jie and Zhigang Liu *

Highly dispersed Co–N–C catalysts were successfully prepared via a defect strategy to anchor metal atoms with a carbon coating. The catalysts showed remarkable catalytic performance under mild conditions (a yield of 97.0% for ethylbenzene oxidation). Meanwhile, BET, TEM, XRD, Raman spectroscopy and XPS studies were employed to investigate the as-prepared catalysts. The results revealed that the unique structure was conducive to producing more defects in carbon, increasing the number of active sites and enhancing the dispersion of cobalt. The outstanding catalytic performance of the catalysts was attributed to the synergy effect of the special structure and the Co–N, pyridine nitrogen and graphite nitrogen species.

 Received 14th January 2020,
 Accepted 9th March 2020

DOI: 10.1039/d0nj00213e

rsc.li/njc

1. Introduction

Hydrocarbon activation and selective oxidation is one of the most important reactions in the modern chemical industry; it is an important method to obtain pharmaceutical and fine chemical intermediates with wide applications.^{1–4} However, its actual application is limited by the low conversion rate of the substrate and the low selectivity of the target product. At present, most of the catalysts used in industrial production are inorganic catalysts or noble metal catalysts; however, they still have many shortcomings. For example, inorganic catalysts are difficult to recover and produce toxic by-products. Moreover, Pt and Pd-based catalysts are costly.^{5–8} Hence, it is of great significance to develop a catalyst for the selective oxidation of hydrocarbons with high performance.

Very recently, it is worth mentioning that transition metals (e.g., Co, Fe, Ni and Mn) supported by nitrogen-doped carbon catalysts (denoted as M–N–C) are one of the most promising alternatives to precious-metal-based catalysts, which is attributed to their excellent performance, abundance, economical applicability and methanol tolerance.^{9–12} However, M–N–C catalysts are currently mostly prepared by high-temperature calcination synthesis, in which the metal precursor, N-containing ligands and carbon source are one-pot calcined at 600–1000 °C in an inert atmosphere. Metal atoms tend to agglomerate at a

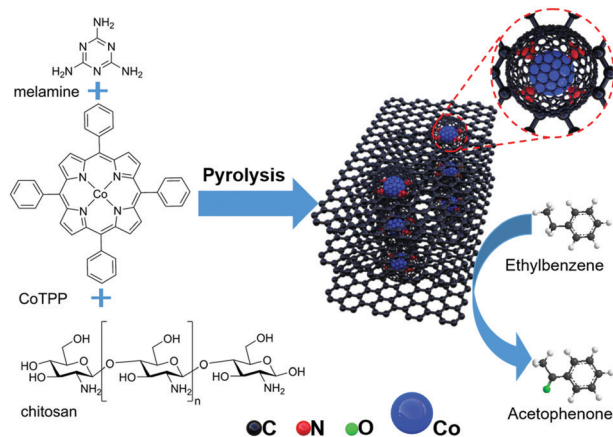
high temperature; thus, the metal particle diameter increases and the distribution of the metal is uneven, which will lead to decreased catalytic performance.¹³ Therefore, it is important to devise an efficient synthesis method to alleviate metal agglomeration when preparing M–N–C catalysts.

It should be noted that the nitrogen in the M–N–C catalysts plays an important part in regulating the properties of materials because nitrogen atoms can provide lone pair electrons to form a delocalized conjugated system.¹⁴ This system can not only change the electronic structure and catalytic properties of the adjacent carbon atoms,¹⁵ but also coordinate with the empty orbital of the transition metal to anchor metal atoms.¹⁶ Recently, for the process of transforming noble metal nanoparticles into thermally stable single atoms *via in situ* environmental transmission electron microscopy, Wei *et al.* found that the defects of nitrogen-doped carbon in an inert atmosphere can capture movable precious metal atoms and disperse metal nanoparticles due to the formation of stable metal–N₄ structures.¹⁷ Inspired by this, we proposed a method to prepare carbon catalysts with highly dispersed metal species based on the defect strategy to anchor metal atoms in nitrogen-doped carbon with a carbon coating.

The specific strategy is shown in Scheme 1. In this project, melamine, the nitrogen-rich material, was used as a nitrogen source to obtain nitrogen-doped carbon. We selected metalloporphyrin, a metallic macrocyclic compound, as the metal precursor; it can limit metal ions to the molecular level so that the metal atoms can be uniformly distributed in the catalyst.¹⁸ A similar metal precursor was reported as an available building block precursor for ORR/OER.¹⁹ On account of the strong coordination ability between chitosan and metal ions, which

State Key Laboratory of Chemo/Biosensing and Chemometrics, College of Chemistry and Chemical Engineering, Hunan University, Changsha, Hunan 410082, China.
 E-mail: liuzhigang@hnu.edu.cn

† Electronic supplementary information (ESI) available: Experimental details, graphics (Fig. S1–S3) and tables (Table S1). See DOI: 10.1039/d0nj00213e



Scheme 1 Schematic of the fabrication process of highly dispersed Co-N-C-X.

is conducive to the formation of coating structures by pyrolysis to slow metal aggregation, we chose this renewable and low-cost resource as the carbon source.²⁰ Co-N-C-X catalysts with small metal particle sizes and high dispersions of Co species were prepared by pyrolysis of mixtures with different amounts of CoTPP, melamine and chitosan at 700 °C. We chose 700 °C as the pyrolysis temperature because the pyrolysis of chitosan and melamine yielded nitrogen-doped carbon graphene sheets at 700 °C,²¹ which facilitated the formation of metal-N₄ structures to anchor metal atoms and thus disperse the active sites. We applied ethylbenzene oxidation as a probe experiment and *tert*-butyl hydrogen peroxide (TBHP) as an oxidant under mild reaction conditions to investigate the performance of the catalysts. Furthermore, the structures and active sites of the prepared catalysts were detected by nitrogen adsorption-desorption isotherms, transmission electron microscopy, X-ray diffraction, Raman spectroscopy and X-ray photoelectron spectroscopy.

2. Experimental section

2.1. Materials

N,N-Dimethyl formamide (DMF), pyrrole, propionic acid, methylene dichloride (CH₂Cl₂), benzaldehyde, cobalt chloride hexahydrate (CoCl₂·6H₂O), ethyl alcohol, melamine and chitosan were commercially available and were used as received without further purification. Deionized (DI) water was homemade.

2.2. Catalyst preparation

2.2.1 Synthesis of cobalt(II) porphyrin. The cobalt(II) 5,10,15,20-tetraphenylporphyrin (CoTPP) was synthesized by referring to a reported technique.²² Freshly distilled pyrrole (2.62 g) mixed with propionic acid (20 mL) was added to a 500 mL three neck flask containing a mixture of benzaldehyde (5.62 g) and propionic acid (200 mL). When the reaction solution turned purple-black, it was refluxed for 1 hour at 130 °C. After adding 100 mL DI water and then cooling overnight, the resulting precipitate was washed with DI water and purified by column chromatography, affording tetraphenyl porphyrin (TPP).

Subsequently, *N,N*-dimethyl formamide (100 mL) was dissolved in 1.0 g of TPP, and CoCl₂·6H₂O (2.5 g, 10.5 mmol) was added to the flask. Then, the mixture was refluxed for 1 hour at 120 °C. After cooling overnight, the final product (CoTPP) was prepared by suction filtration, washing and drying in turn.

2.2.2 Preparation of Co-N-C and related composites. The Co-N-C catalyst was synthesized from chitosan, melamine and cobalt porphyrin, which acted as the carbon source, nitrogen source and metal precursor, respectively. In the process of synthesis, after adding CoTPP (*X* mg, *X* = 5, 10, 20, 50, or 100), ethyl alcohol (20 mL), chitosan (0.2 g) and melamine (0.8 g) were added to a 50 mL round-bottomed flask and maintained with ultrasonic dispersion for half an hour; then, the mixture was refluxed with magnetic stirring at 60 °C for 3 h. Following that, ethyl alcohol was removed by a rotary evaporator, and the obtained solid was dried in an oven at 80 °C for 8 h. Subsequently, the solid was ground into fine powder. The powder was loaded into a corundum boat and heated in N₂ atmosphere at 700 °C for 2 h. The final product was denoted as Co-N-C-*X* (*X* = 5, 10, 20, 50, or 100). The reference samples, including N-C (without CoTPP), Co-MEL-20 (without chitosan), Co-CTS-20 (without melamine) and CoCl₂-N-C (replacing CoTPP with 7.1 mg of CoCl₂·6H₂O), were prepared *via* similar methods.

2.3. Tests of catalytic performance

We explored the catalytic capacity *via* the selective oxidation of hydrocarbon under mild conditions as a probe experiment. In the measurements, after 15 mg of catalyst and DI water (3 mL) were added in that order, the substrate (1.0 mmol) and TBHP (3.5 mmol, 70 wt% in water) were injected into the reaction tube by a pipette. The reaction was then maintained at 80 °C for 12 h, accompanied by magnetic stirring. Following that, GC analysis was applied to quantitatively detect the sample extracted with ethyl acetate (9 mL), using *n*-dodecane (100 μL) as an internal standard. Meanwhile, the catalyst was recycled for the next run, denoted as Co-N-C-*X*-R₂ (*X* = 5, 10, 20, 50, 100), and Co-N-C-*X*-R₃ were obtained by the same logic.

3. Results and discussion

3.1. TEM

We carried out TEM and element mapping to determine the morphology and microstructure of the Co-N-C-20 composite. As shown in Fig. 1a, the surface topography characteristics of crumpled and stacked graphene nanosheets were observed in Co-N-C-20. In addition, the TEM diagram of Co-N-C-20 (Fig. 1b) showed uniformly dispersed black spots, which were the coating structure formed by the carbonized chitosan coated on cobalt atoms. It was reported by Beller's group that a carbon coating structure can provide catalytic active sites.²³ This result was consistent with the structure model of the catalyst we proposed above. We did not find a metal lattice in Fig. 1d; this may be because the carbon-coated sandwich structure based on defect anchoring resulted in highly dispersed cobalt nanoclusters. However, the well-dispersed cobalt species were also illustrated

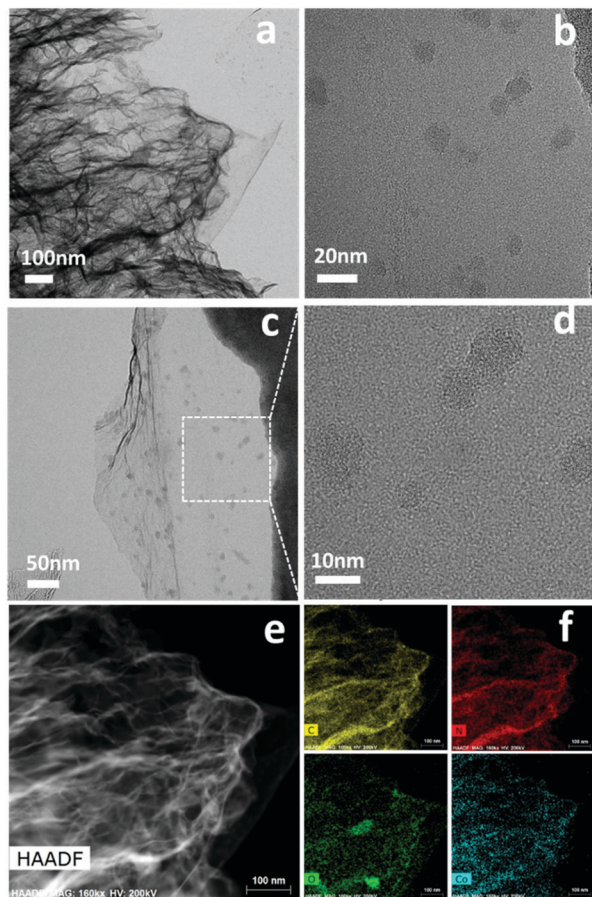


Fig. 1 (a–d) TEM images of Co–N–C–20 at various resolutions, (e) and (f) HAADF–STEM images and corresponding element maps of the Co–N–C–20 catalyst.

in the element mapping (Fig. 1f). Furthermore, the element mapping diagram of cobalt was in good agreement with the nitrogen mapping (Fig. 1f), proving that the defects of nitrogen-doped carbon could immobilize cobalt atoms and that the cobalt atoms were successfully combined with nitrogen.

3.2. Raman and XRD

To further investigate the graphitization process and heteroatomic defects of Co–N–C–X (Fig. 2a), Raman spectroscopy was conducted. An obvious D band at about 1347 cm^{-1} (associated with defects induced by heteroatom doping) and a G band at about 1578 cm^{-1} (corresponding to graphitic carbon) were obtained in the Raman spectra.^{24,25} Generally, the comprehensive intensity ratio of the D band *versus* the G band (I_D/I_G) is a significant parameter to study the characteristics of carbon materials, reflecting the defect level in the graphitic carbon layers. As reported in some research, carbon materials with high I_D/I_G ratios are regarded to have more structure defects, which can enhance the performance of catalysts.²⁶ For Co–N–C–5, Co–N–C–20, *etc.*, the increase of CoTPP content led to an increase of I_D/I_G ; this revealed that the overlapping of melamine, CoTPP and chitosan synergistically facilitated the generation of heteroatomic defects from cobalt and nitrogen in

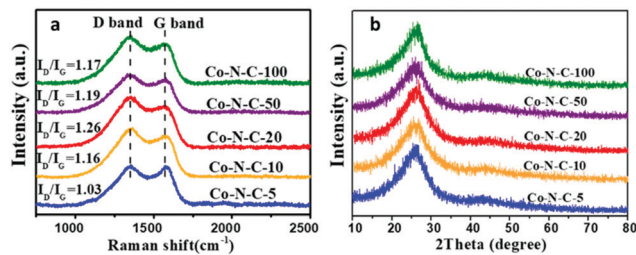


Fig. 2 Raman spectral analysis and XRD analysis of Co–N–C–X ($X = 5, 10, 20, 50, 100$).

the catalyst. Among all these Co–N–C–X materials, Co–N–C–20 possessed the highest I_D/I_G ratio, indicating that Co–N–C–20 had the highest defect content. Meanwhile, with respect to Co–N–C–20, Co–N–C–100, *etc.*, the decrease of I_D/I_G demonstrated clearly that the planar extension of ideal graphene layers increased.²⁷ The changing trends of the Raman spectra agreed with the catalytic activity of the catalysts (Table 2), which confirmed that the defects had an impact on the catalytic performance of the catalysts.

X-ray diffraction (XRD) was carried out to study the crystal-line structure of Co–N–C–X ($X = 5, 10, 20, 50, 100$), as demonstrated in Fig. 2b. The XRD patterns of all the samples revealed a broad peak at 26° , which was attributed to the diffraction peak of the (002) plane of graphene sheets.²⁸ This coincided with the TEM results (Fig. 1a). Unsurprisingly, peaks of metallic cobalt were not detected in the XRD patterns of Co–N–C–X ($X = 5, 10, 20, 50, 100$); this is probably due to the small size and high dispersion of cobalt in the nitrogen-doped carbon.²⁹ This result verified that the strategy adopted in this study was conducive to achieving the synthesis of catalysts with well-dispersed cobalt.

3.3. BET

Nitrogen adsorption/desorption measurements were completed at 77 K to characterize the porous properties of the samples. As shown in Fig. 3b, the isotherm is similar to type IV and H3 hysteresis loops in the IUPAC classification; this indicates that the mesoporous structure originates from molecular stacking, which is consistent with the carbon-coated sandwich structure.^{30,31} The specific surface areas (Table 1) and pore diameter distributions (Fig. 3a) of the samples were in line with the results of the Raman analysis, explaining that the carbon-coated sandwich structure was favourable to increase the specific surface area.

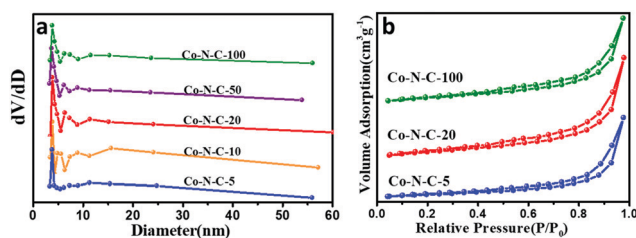


Fig. 3 (a) Pore size distributions of Co–N–C–X ($X = 5, 10, 20, 50, 100$), (b) nitrogen adsorption–desorption isotherms of Co–N–C–X ($X = 5, 20, 100$).

Table 1 The results of the N₂ adsorption–desorption measurements

Sample	S_{BET}^a (m ² g ⁻¹)	V_{tot}^b (cc g ⁻¹)	D_p^c (nm)
Co–N–C-5	37.7	0.19	20.5
Co–N–C-10	39.3	0.15	18.2
Co–N–C-20	39.3	0.13	14.3
Co–N–C-50	36.7	0.12	13.7
Co–N–C-100	27.1	0.09	13.3

^a Surface areas calculated using the BET method. ^b Total pore volumes estimated from the N₂ adsorption isotherm at $P/P_0 = 0.98$. ^c Mesopore diameters calculated from the N₂ desorption branches using the BJH method.

3.4. XPS

In order to further investigate the chemical states and surface compositions of the N, C, and Co species in the catalysts, we carried out X-ray photoelectron spectroscopy (XPS) measurements. In Fig. 4a, the elements of Co, C, N and O are displayed in the full survey spectra of Co–N–C-*X*, revealing the relative contents of these elements and the changing trend with increasing cobalt porphyrin content. Meanwhile, the peak of C 1s is highest in Fig. 4a, indicating that the relative contents of C were highest in these catalysts. The high-resolution C 1s spectrum (Fig. 4b) showed three peaks at 284.6 eV, 286.0 eV, and 288.4 eV, which were assigned to C=C, C–N and O–C=O, respectively.^{31,32} The O 1s spectrum (Fig. 4c) can be deconvoluted into two peaks centred at binding energies of 531.1 eV and 532.3 eV; these were assigned to carboxyl and hydroxyl groups, respectively.³³ The N 1s spectrum (Fig. 4d) presented four different configurations of N species, including pyridinic N (N1, 398.3 eV), pyrrolic N (N2, 399.1 eV), graphitic N (N3, 400.6 eV) and *N*-oxides (N4, 403.5 eV).^{28,34} As reported in some research, not only can pyridine N coordinate with metal ions (Co–N), giving rise to high catalytic activity, but graphitic N can also be an active specie to promote the oxidation reactions of alkanes and alcohols.^{35,36} The scale of pyridinic N and graphitic N (total of 86.70%) in the Co–N–C-20 catalyst was higher than those in the

Co–N–C-100 (total of 75.00%) and Co–N–C-5 (total of 59.93%) catalysts (Table S1, ESI†). Meanwhile, the catalytic performance of Co–N–C-20 was better than those of the other samples, revealing that pyridinic N and graphitic N may exert influences on ethyl benzene oxidation.

It is worth noting that the content of Co species in Co–N–C-20 was not the highest; however, it possessed the highest content of Co 2p_{3/2}. Thus, the Co 2p XPS spectra were acquired to further explore the chemical structures of cobalt element in the samples. As shown in Fig. 4e, the peaks with representative binding energies of 780.2 eV and 796.2 eV can clearly be seen, corresponding to the Co 2p_{3/2} and Co 2p_{1/2} electrons; meanwhile, the peaks at 786.3 eV and 802.2 eV are shake-up satellite peaks. The high-resolution spectrum of Co 2p_{3/2} revealed a distribution of Co 2p_{3/2} in two species: Co–O and Co–N, observed at 780.6 eV and 782.7 eV, respectively.^{28,37,38} From Co–N–C-5 to Co–N–C-20, the increase of CoTPP content leads to an increase of Co–N and a decrease of Co–O, indicating that the carbon-coated sandwich structure based on defect anchoring promoted the formation of Co–N (Table S1, ESI†). However, the proportion of Co–N in Co 2p_{3/2} of Co–N–C-100 was reduced; this may be because agglomeration of surplus cobalt destroyed the bonds of Co–N so that more Co–O bonds were formed.³⁹

3.5. Performance of the catalysts

Acetophenone is a significant chemical material that is used to make perfume and as an intermediate in organic synthesis. Catalytically selective oxidation of ethylbenzene is a feasible method for the preparation of acetophenone with good practical prospects.⁴⁰ Hence, the selective oxidation of ethylbenzene with TBHP as an oxidant and water as a solvent was selected as the probe reaction to evaluate the catalytic properties of the as-prepared catalysts (Table 2). Co–MEL-20 (without chitosan, conv. 57.5%), Co–CTS-20 (without melamine, conv. 29.8%) and N–C (without cobalt, conv. 55.9%), as contrast samples, exhibited poor catalytic activity, proving that three different raw materials were essential to the special structure of these catalysts. It is necessary to note that Co–CTS-20 (less nitrogen, sel. 72.1%) and N–C (without cobalt, sel. 84.4%) showed lower selectivity than the other samples, indicating that Co–N is the main active site of the selective oxidation of ethylbenzene. However, CoCl₂–N–C (conv. 86.1%), with the same molar amount of cobalt as Co–N–C-20, afforded lower ethylbenzene conversion than Co–N–C-20, possibly because the macrocyclic structure of cobalt porphyrin is beneficial to the high dispersion of cobalt atoms.¹⁸ The influence of the cobalt porphyrin content on the catalytic performance was explored in order to further verify the active sites of Co–N–C-*X*. With increasing amount of cobalt porphyrin content in the Co–N–C-*X* catalysts, the change trend of Co–N content was identical to the change trend of ethylbenzene conversion (Table S1, ESI† and Table 2), suggesting once more that the Co–N bond is the active site in Co–N–C-*X* for the selective oxidation of ethylbenzene. The catalytic capability decreased from Co–N–C-20 to Co–N–C-100 (Table 2, entries 7–9), possibly due to aggregation of redundant cobalt atoms.³⁹ Interestingly, the decline in activity was slow,

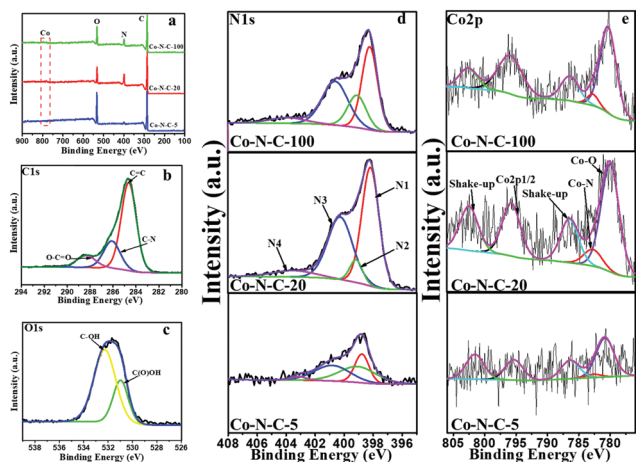
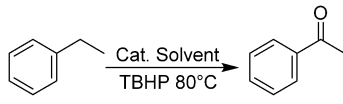


Fig. 4 XPS spectra of the as-prepared catalysts. (b) C 1s XPS spectrum and (c) O 1s XPS spectrum of the sample Co–N–C-20; (a), (d) and (e) XPS survey spectra, N 1s and Co 2p XPS spectra of Co–N–C-100, Co–N–C-20 and Co–N–C-5.

Table 2 Catalytic performance of the catalysts for ethylbenzene oxidation

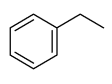
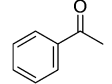
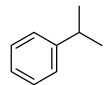
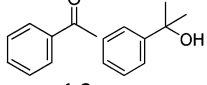
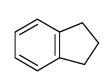
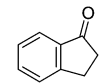
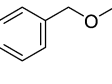
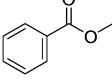
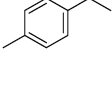
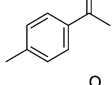
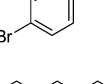
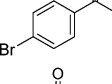
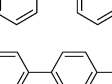
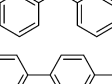
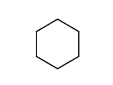
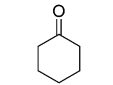
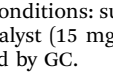
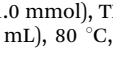


Entry	Catalyst	Conv./%	Sel./%
1	CoCl ₂ -N-C	86.1	98.1
2	Co-MEL-20	57.5	92.0
3	Co-CTS-20	29.8	72.1
4	N-C	55.9	84.4
5	Co-N-C-5	74.8	95.4
6	Co-N-C-10	81.7	96.9
7	Co-N-C-20	97.0	99.6
8	Co-N-C-50	93.7	98.8
9	Co-N-C-100	89.0	97.3
10	Co-N-C (800)	90.9	99.3
11	Co-N-C-20-R ₂	84.1	95.2
12	Co-N-C-20-R ₃	75.0	92.2

Reaction conditions: ethylbenzene (1.0 mmol), TBHP (3.5 mmol, 70 wt% in water), catalyst (15 mg).

illustrating that the carbon-coated sandwich structure can weaken the aggregation of metal ions to some extent. Meanwhile, Co-N-C-20 (conv. 97.0%), with higher catalytic competence than the others, was attributed to the higher content of Co-N

Table 3 Catalytic oxidation of several substrates by Co-N-C-20

Entry	Substrate	Product	Conv./%	Sel./%
1			97	99.6
2		 1:2	94.1	98.45
3			> 99	46.14
4			> 99	63.7
5			90	89.12
6			97.5	> 99
7			> 99	> 99
8			> 99	> 99
9			95.9	70.1

Reaction conditions: substrate (1.0 mmol), TBHP (3.5 mmol, 70 wt% in water), catalyst (15 mg), H₂O (3 mL), 80 °C, 12 h; the conversion was determined by GC.

bonds and greater number of defects according to the analysis of the XPS and Raman measurements. Actually, the pyrolysis temperature has a great influence on the performance of the catalysts; for example, high temperature is conducive to the reduction of cobalt.⁴¹ We prepared Co-N-C (800) at the pyrolysis temperature of 800 °C, in which the other conditions were the same as for the synthesis of Co-N-C-20. We found that the catalytic capacity of Co-N-C (800) (conv. 90.9%, sel. 99.3%) was lower than that of Co-N-C-20 because the higher surface energy of cobalt at 800 °C led to more metal agglomeration.⁴² However, the yield of Co-N-C (800) for ethylbenzene oxidation was still approximately 90%, indicating that our strategy can be useful at higher temperatures.

Afterwards, we investigated the catalytic performance of Co-N-C-20 for the oxidation of other hydrocarbons, as shown in Table 3. Delightfully, the conversions of the examined hydrocarbons were all good; this shows that Co-N-C-20 possesses a certain level of universality for the catalytic oxidation of hydrocarbons, especially hydrocarbons with two phenyl groups (Table 3, entries 7 and 8). It also suggests that Co-N-C-20 can facilitate the activation of C-H bonds. Moreover, compared with the conversion of *p*-ethyltoluene and *p*-bromoethylbenzene (Table 3, entries 5 and 6), we found that hydrocarbons with electron withdrawing groups were more likely to be oxidized.

4. Conclusion

In summary, we successfully prepared highly dispersed metal nanocluster catalysts *via* a defect strategy to anchor metal atoms with a carbon coating. Among these catalysts, Co-N-C-20 not only possessed superior catalytic capacity of selective ethylbenzene oxidation, but also had high catalytic activity for other substrates; this indicates that it possesses wide applicability. Based on a series of control group experiments and characterization results, we discovered that the excellent catalytic performance of the catalyst is probably due to synergy effects of the special structure, Co-N bonds, and pyridine nitrogen and graphite nitrogen species. This new integrated strategy may provide an additional method for future research.

Conflicts of interest

There are no conflicts to declare.

Acknowledgements

This work was supported by the National Natural Science Foundation of China (No. 21872045).

Notes and references

- 1 A. E. Shilov and G. B. Shul'pin, *Chem. Rev.*, 1997, **97**, 2879–2932.
- 2 L. Kesavan, R. Tiruvalam and M. H. A. Rahim, *Science*, 2011, **331**, 195–199.

- 3 H. Liu, G. Chen, H. Jiang, Y. Li and R. Luque, *ChemSusChem*, 2012, **5**, 1892–1896.
- 4 S. Pendem, R. Singuru, C. Sarkar, B. Joseph, J. F. Lee, D. B. Shinde, Z. Lai, J. Mondal and A. C. S. Appl, *Nano Mater.*, 2018, **1**, 4836–4851.
- 5 D. Yang, T. Jiang, T. Wu, P. Zhang, H. Han and B. Han, *Catal. Sci. Technol.*, 2016, **6**, 193–200.
- 6 U. Neuenschwander and I. Hermans, *J. Org. Chem.*, 2011, **76**, 10236–10240.
- 7 V. R. Choudhary, J. R. Indurkar, V. S. Narkhede and R. Jha, *J. Catal.*, 2004, **227**, 257–261.
- 8 Q. Yang, W. Wang, Y. Zhao, J. Zhu, Y. Zhu and L. Wang, *RSC Adv.*, 2015, **5**, 54978–54984.
- 9 W. Liu, L. Zhang, X. Liu, X. Yang, S. Miao, W. Wang, A. Wang and T. Zhang, *J. Am. Chem. Soc.*, 2017, **139**, 10790–10798.
- 10 X. X. Wang, D. A. Cullen, Y. T. Pan, S. Hwang, M. wang, Z. Feng, J. Wang, M. H. Engelhard and G. Wu, *Adv. Mater.*, 2018, **30**, 1706758.
- 11 R. Nie, J. Chen, M. Chen, Z. Qi, T. Y. Goh, T. Ma, L. Zhou, Y. Pei and W. Huang, *Green Chem.*, 2019, **21**, 1461–1466.
- 12 J. Li, J. Zhang, S. Wang, G. Xu, H. Wang and D. G. Vlachos, *ACS Catal.*, 2019, **9**, 1564–1577.
- 13 P. R. Jothi, K. Yubuta and B. P. T. Fokwa, *Adv. Mater.*, 2018, **30**, 1704181.
- 14 Y. Y. Chu, J. Gao, Z. Tao and X. Y. Tan, *J. Mater. Chem. A*, 2014, **2**, 4038–4044.
- 15 T. Y. Ma, S. Dai, M. Jaroniec and S. Z. Qiao, *Angew. Chem., Int. Ed.*, 2014, **53**, 7281–7285.
- 16 Z. Chen, J. Zhao, C. R. Cabrera and Z. Chen, *Small Methods*, 2018, 1800368.
- 17 S. Wei, A. Li, J. C. Liu, Z. Li, H. Xiao, C. Chen, J. Li and Y. Li, *Nat. Nanotechnol.*, 2018, **13**, 856.
- 18 Y. Jiao, Y. Zheng, M. Jaroniec and S. Z. Qiao, *Chem. Soc. Rev.*, 2015, **44**, 2060–2086.
- 19 H. Li and Z. Sui, *New J. Chem.*, 2019, **43**, 17963–17973.
- 20 B. Sahoo, A. E. Surkus, M. M. Pohl and J. Radnik, *Angew. Chem., Int. Ed.*, 2017, **129**(37), 11394–11399.
- 21 M. K. Rybarczyk, M. Lieder and M. Jablonska, *RSC Adv.*, 2015, **5**(56), 44969–44977.
- 22 C. Shen, S. S. Jie, H. Chen and Z. G. Liu, *Front. Chem.*, 2019, **7**, 426.
- 23 F. A. Westerhaus, R. V. Jagadeesh, G. Wienhöfer, M. M. Pohl, J. Radnik, A. E. Surkus, J. Rabeah, K. Junge, H. Junge, M. Nielsen, A. Brückner and M. Beller, *Nat. Chem.*, 2013, **5**, 537–543.
- 24 C. Guo, W. Liao, Z. Li, L. Sun and C. Chen, *Nanoscale*, 2015, **7**, 15990–15998.
- 25 M. Fan, C. Zhu, Z. Q. Feng, J. Yang, L. Liu and D. Sun, *Nanoscale*, 2014, **6**, 4882–4888.
- 26 X. Lin and S. Jie, *Mol. Catal.*, 2018, **455**, 143–149.
- 27 L. Fu, Y. Chen, S. Zhao, Z. Liu and R. Zhu, *RSC Adv.*, 2016, **6**, 19482–19491.
- 28 X. Lin, R. Zhu, Z. Liu, S. Zhao and L. Fu, *J. Mol. Catal. A: Chem.*, 2016, **420**, 11–17.
- 29 Y. Chen, S. Jie and C. Yang, *Appl. Surf. Sci.*, 2017, **419**, 98–106.
- 30 T. P. Fellinger, F. Hasché, P. Strasser and M. Antonietti, *J. Am. Chem. Soc.*, 2012, **134**, 4072–4075.
- 31 L. Fu, Y. Chen and Z. G. Liu, *J. Mol. Catal. A: Chem.*, 2015, **408**, 91–97.
- 32 Y. Su, Y. Zhu, H. Jiang, J. Shen, X. Yang, W. Zou and C. Li, *Nanoscale*, 2014, **6**, 15080–15089.
- 33 Z. Ma, H. Zhang, Z. Yang, G. Ji, B. Yu, X. Liu and Z. Liu, *Green Chem.*, 2016, **18**(7), 1976–1982.
- 34 D. Li, Z. Zong, Z. Tang, Z. Liu, S. Chen and Y. Tian, *ACS Sustainable Chem. Eng.*, 2018, **6**, 5105–5114.
- 35 J. Wei, Y. Hu, Z. Wu, Y. Liang, S. Leong, B. Kong, X. Zhang, G. P. Simon and H. Wang, *J. Mater. Chem. A*, 2015, **3**, 16867–16873.
- 36 Y. Gao, G. Hu, J. Zhong, J. Wang, D. S. Su and D. Ma, *Angew. Chem., Int. Ed.*, 2013, **52**, 2109–2113.
- 37 R. V. Jagadeesh, H. Junge, M. M. Pohl and M. Beller, *J. Am. Chem. Soc.*, 2013, **135**, 10776–10782.
- 38 H. S. Lu, H. Zhang, R. Liu, X. Zhang, H. Zhao and G. Wang, *Appl. Surf. Sci.*, 2017, **392**, 402–409.
- 39 E. Bayram, J. Lu, C. Aydin, N. D. Browning, E. Finney and R. G. Finke, *ACS Catal.*, 2015, **5**, 3514–3527.
- 40 C. Ricca, F. Labat, N. Russo, C. Adamo and E. Sicilia, *J. Phys. Chem. C*, 2014, **118**, 12275–12284.
- 41 X. Lin, Z. Nie, L. Zhang, S. Mei, Y. Chen, B. Zhang, R. Zhu and Z. Liu, *Green Chem.*, 2017, **19**(9), 2164–2173.
- 42 R. Qin, P. Liu, G. Fu and N. Zheng, *Small Methods*, 2018, **2**(1), 1700286.